PCCP

Rubrene Single Crystal Solar Cells and the Effect of Crystallinity on Interfacial Recombination

Journal:	*Physical Chemistry Chemical Physics*
Manuscript ID	CP-ART-02-2022-000985.R1
Article Type:	Paper
Date Submitted by the Author:	21-Mar-2022

Complete List of Authors:	Akın Kara, Duygu; Ege University, SOLAR ENERGY INSTITUTE burnett, Edmunt; UMass Amherst Kara, Koray; Selcuk Universitesi, usluer, ozlem; UMass Amherst Cherniawski, Benjamin; University of Massachusetts Amherst, Polymer Science and Engineering Barron, Edward; Virginia Tech Gültekin, Burak; Ege University, Solar Energy Institute Kus, Mahmut; Natural sciences, Briseno, Alejandro; UMass Amherst

ARTICLE

Rubrene Single Crystal Solar Cells and the Effect of Crystallinity on Interfacial Recombination

Received 00th January 20xx,
Accepted 00th January 20xx

DOI: 10.1039/x0xx00000x

Duygu Akin Kara*[ab‡], Edmund K. Burnett[a], Koray Kara[ac], Ozlem Usluer[a], Benjamin P. Cherniawski[a], Edward J. Barron III[a], Burak Gultekin[b], Mahmut Kus[d], and Alejandro L. Briseno*[ae]

Single crystal studies provide a better understanding of the basic properties of organic photovoltaic devices. Therefore, in this work, rubrene single crystals with a thickness of 250 nm to 1000 nm were used to produce an inverted bilayer organic solar cell. Following, polycrystalline rubrene (orthorhombic, triclinic) and amorphous bilayer solar cells of the same thickness as single crystal was studied to make comparisons across platforms. To investigate how single crystal, polycrystalline (triclinic-orthorhombic) and amorphous forms alter the charge carrier recombination mechanism at the rubrene/PCBM interface, light intensity measurements were carried out. Light intensity dependency of JSC, VOC and FF parameters in organic solar cells with different forms of rubrene. Monomolecular (Shockley Read Hall) recombination is observed in devices employed amorphous and polycrystalline rubrene in addition to bimolecular recombination whereas single crystal device is weakly affected by trap assisted SRH recombination due to reduced trap states at the donor acceptor interface. To date, the proposed work is the only systematic study examining transport and interface recombination mechanisms in organic solar cells produced by different structure forms of rubrene.

1. Introduction

Organic semiconductor single crystals are powerful tools for probing the intrinsic properties of materials and provide a way to improvement in the steady electronic device operation[1]. To study charge transport mechanism and achieve a high performance-device, the single crystals can be operated as a prototype model since they have regular shape, almost no grain boundaries, dislocations, or defects[2-3]. Their high mobilities and outstanding electrical characteristics would make them promising candidates for optoelectronic applications such as organic field effect transistors (OFET), phototransistors, pn heterojunctions and electronic circuits as drivers for active matrix displays and sensor arrays[4-5]. Yet, for all their work in the field of organic electronics, there are few examples of them being utilized in photovoltaic studies due to processing difficulties. Rubrene (5,6,11,12 – tetraphenyltetracene; $C_{42}H_{28}$), a benchmark semiconductor, has exhibited one of the highest mobilities (40 $cm^2/V.s$) in the single crystal form and a very commonly employed material for studying interactions of external stimuli with organic semiconductors[6]. For instance, rubrene single crystal based OFETs have been extensively examined regarding the charge transport mechanism, anisotropic and mechanical properties. On the other hand, solar cell studies with rubrene organic single crystals are limited due to their hard handling process, fragile and poor processability properties cause some difficulties for device fabrication. Recently one of the outstanding studies on rubrene single crystal solar cell is the study of Karak et al., which investigated the intrinsic interface properties of ITO/rubrene single crystal/Al in lateral Schottky devices[7]. Although, charge carrier mobility of rubrene thin film form is not so good because of poor crystallinity[8], detailed understanding of its processing conditions allow to fabricate very well controlled polycrystalline films[9]. Exploiting the epitaxial growth of rubrene onto thin film enabled the first fabrication of a polycrystalline photovoltaic device[10]. There are some studies to examine the effect of different crystal phases formed using different annealing temperatures on charge transfer states. Amassian et al. have shown that how structural heterogeneities of rubrene thin film effect the CT state and V_{oc} in conventional solar cell[11]. However, there is still a significant lack of studies on the systematic variation from amorphous, semi-crystalline and single crystal forms of rubrene based organic solar cell and effects on interfacial transport mechanism. In this study, we first, have fabricated inverted organic photovoltaic devices using rubrene single crystals and investigated device performance as a function of crystal thickness. Then, comparisons were made between platforms by producing polycrystalline orthorhombic, triclinic, and amorphous devices with the same thickness as the single crystal. To investigate how single crystal and amorphous/polycrystalline forms affect the charge carrier transport at the rubrene/PCBM interface, we have realized light

[a.] Department of Polymer Science and Engineering, University of Massachusetts Amherst, Amherst, MA, 01003, USA
[b.] Solar Energy Institute, Ege University, 35000, Izmir, Turkey Address here.
[c.] Izmir Graphene Application and Research Center, Izmir Katip Celebi University, 35000, Izmir, Turkey
[d.] Department of Chemical Engineering, Konya Technical University, 42000, Konya, Turkey
[e.] US NAVY, NAWCWD, Research Office, China Lake, California 93555, United States
Electronic Supplementary Information (ESI) available: [details of any supplementary information available should be included here]. See DOI: 10.1039/x0xx00000x

intensity measurements, providing comprehensive information on bulk or interface recombination. To the best of our knowledge, recombination mechanism in terms of monomolecular and bimolecular recombination and detailed solar cell device performance have not been investigated to across platforms from the single crystalline to amorphous form of rubrene in inverted bilayer organic solar cells.

2. Experimental Section

2.1. Rubrene Crystal Growth

Physical vapor transport (PVT) system was used to fabricate rubrene single crystals. Commercially available rubrene powder (Acros Organics-Purity with 99.99%) which is used as the source material, was placed on a cleaned glass sleeve inside the PVT system. Thin rubrene single crystals could be grown by fast sublimation rate condition which is the source temperature was ~330 °C under inert gas (argon) flow with a rate about 100 mL/min. Zeiss AxioCam ICc1 camera were used to obrained the optical microscope images.

2.2. Solar Cell Fabrication

Commercially available ITO-coated glasses were used as a substrate. After usual cleaning process (15 min water, acetone, and isopropanol), substrates were exposed to UV-ozone treatment to activate the surfaces for 3 minutes. C60-N which is dissolved in 2,2,2-Trifluoroethanol (TFE) 0.4 %, was deposited onto ITO glasses as interlayer by spin coating at 4000 rpm for 30 s and annealled 75 °C for 5 min. After that, PCBM solution, which is dissolved in chlorobenzene 0.5 wt %, was spin-coated as an electron transport layer at 4000 rpm for 40 s and annealed 80 °C for 5 min to evaporate residual solvents. Rubrene single crystals have placed onto PCBM coated surface by using PDMS (polydimethylsiloxane) stamp was used to raise adhesion between crystal and PCBM surface. The thicknesses of C60-N and PCBM layers are 15 nm and 35 nm, respectively. Finally,100 nm Ag (99.99% purity) and 8 nm MoO_3 which is was reported as a electron blocker, thermally evaporated as anode electrodes by a glovebox-integrated PVD system.

2.3. Device Characterizations

All measurements were completed in a MBraun M200 glovebox system under nitrogen atmosphere. A glovebox-integrated Newport solar simulator used as an AM1.5 light source. Photocurrent and voltage characterization were done by a Keithley 4200 source meter. The absorption spectra were recorded with a Shimadzu UV-3600 Spectrophotometer. The optical microscopy (Zeiss Axiovert 200M, 5x or 10x objective, CCD camera) with ImageJ was used to get single crytsal opticam images. Crystal thickness was obtained using an optical profilometer (Zygo NewView 7300, Veeco DekTak 150, and Veeco NT9080) The XRD experiments were conducted by a Panalytical Empyrean X-ray diffractometer. The surface morphology of rubrene films was examined using tapping mode AFM (Ambios technology).

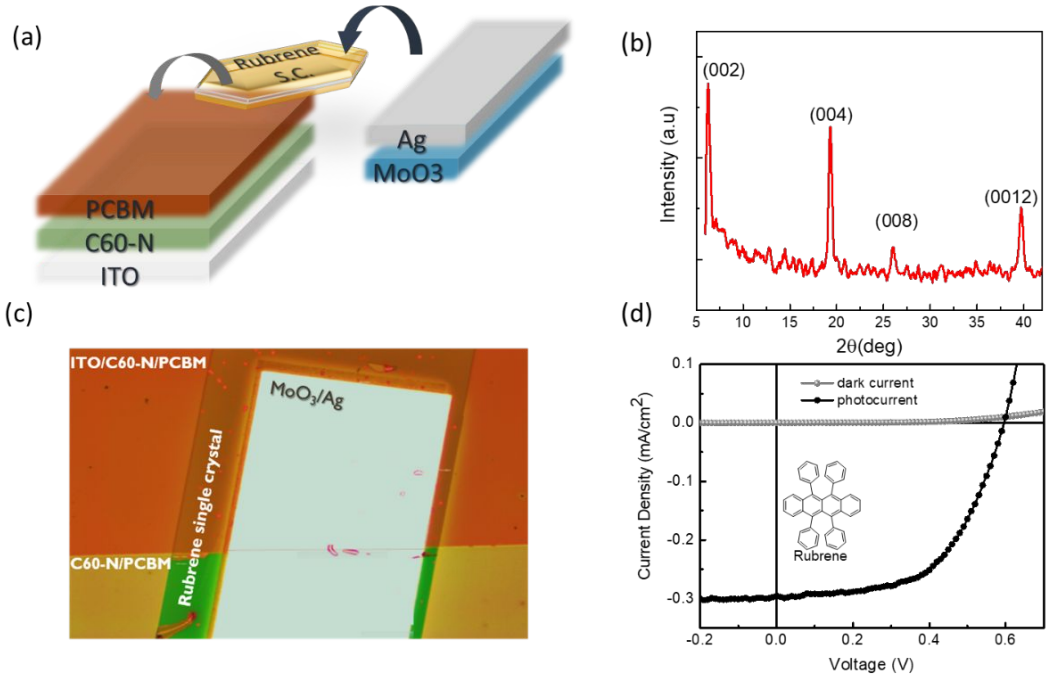

Figure 1. (a) Schematic illustration of the inverted bilayer device structure (b) XRD pattern of rubrene single crystal, (c) optical microscope image of the rubrene single crystal solar cell, (d) Current density – voltage characteristics of rubrene single crystal solar cell in the dark and under illumination

3. Results and Discussions

The schematic of the single-crystal solar cell is shown in **Figure 1a**. Rubrene is selected donor to fabricating working inverted bilayer organic solar cell. The device structure comprised of a C_{60}-N (fulleropyrrolidines with amine) interlayer coated ITO substrate. PCBM (Phenyl-C61-butyric acid methyl ester) is selected acceptor which is commonly used solution processed form. PCBM film was then spin coated, as it created better adherence with rubrene crystal than C_{60}-N. A 250 nm rubrene single crystal was then placed onto the PCBM film. This type of crystals (with thicknesses below 1 micron) are naturally bendable and bond the PCBM surface through Van der Waals forces. The XRD pattern of Rubrene single crystal produced by PVT (Physical vapor transport) method is shown in **Figure 1b**. The diffraction peaks are sharp and peak at 6.55˚ corresponding with (002) crystal plane and other equivalent periodic peaks with high intensity corresponding to (004), (008) and the others also convenient with literature[12]. An optical image of the completed single-crystal device is shown in **Figure 1c**. The dark and illuminated current voltage characteristics of rubrene single crystal solar cell can be seen **Figure 1d**. Under solar illumination equivalent to one sun, the champion device exhibited a short-circuit current density (J_{SC}) of 0.30 mA/cm^2, an open-circuit voltage (V_{OC}) of 0.60 V, a fill factor of 0.57 and the resulting PCE of 0.10 %. In there, notable difference between the dark current density and the photogenerated current density at $V>V_{OC}$ could be explained by electronic doping mechanism which is originated from asymmetrical impurities (or defect levels) between donor (Rubrene Single crystal/no impurities) and acceptor (PCBM thin film) layers[13]. A variety of single-crystal devices were fabricated to investigate the effect of crystal thickness on PCE. Devices tested ranged from 250 nm to 1000 nm, with PCE decreasing from 0.1 % at 250 nm to 0.01 % at 1000 nm. **Table S1** shows the illuminated solar cell device parameters as a function of crystal thickness. As can be shown in **Figure 2**, the V_{OC} has not showed the big dependence on the crystal thickness since they have similar photovoltaic properties in terms of energy levels. In additon, in devices with thicker crystals, slight Voc drops could be related by charge recombination[14]. The small dependence of FF on crystal thickness can be explained by better cohesion of thinner crystals. J_{SC} is relatively sensitive to thickness compared to decrease in V_{OC} and FF, which reduced from 0.3 mA/cm^2 at 250 nm to 0.062 mA/cm^2 at crystal thicknesses of 1000 nm. This results also confirmed by the serial resistance results calculated from dark current voltage graph which increased more than one order of magnitude, from 18 Ω cm^2 to 205 Ω cm^2 for 250 nm and 1000 nm, respectively. This performance decrease could be caused by the difference in flexibility of the thin and thick crystals, as the thin crystals better adhered and conformed to the substrate, creating pin hole free interface. The optical microscope images of varied thickness of rubrene single crystals can be seen in Figure S1. In there, thicker crystals have not adhered to surface properly giving rise to detrimental interface

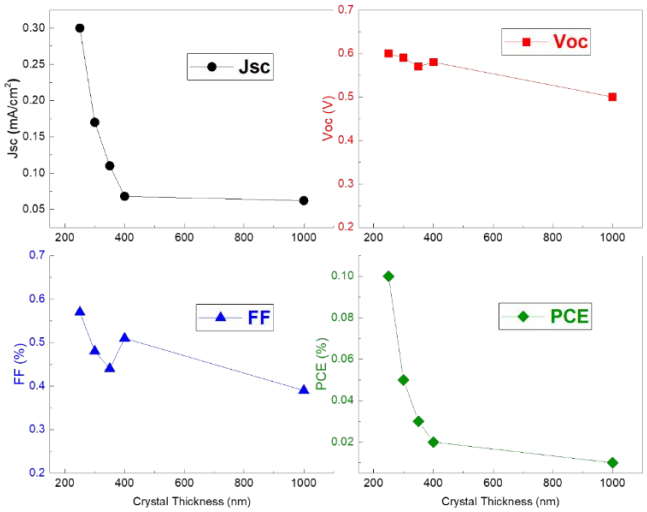

Figure2. Rubrene single crystal solar cell characteristics as a function of crystal thickness: short-circuit current density (JSC), open-circuit voltage (VOC), fill factor (FF), and power conversion efficiency (PCE).

for solar cell operation. In addition to adhesion problems, the J_{SC} decreasing could be explained with in two ways: 1- incident excitation light intensity reduced with increasing crystal thickness[15] (especially up to 500 nm) which is limiting density of photogenetared carriers and 2- the thicker crystals are larger than the exciton diffusion length supressing charge collection compared with thinner crystals. Also, there is another distintion between photocurrents of thin (L=250 nm) and thick (L=1000 nm) crystals could be coming from space charge effects, since photogenerated holes need to transit longer pathway than drift lengths in thick crystal paving the pay for charge carrier recombination[16]. These reasons could be an evidence of big J_{SC} drop for solar cells with 1000 nm rubrene single crystal. Nevertheless, this reduced performance is much less than previous studies using tetracene single crystals in which PCE decreased by three orders of magnitude when crystal thickness was varied over a similar range[17]. This could be caused by larger exciton diffusion lengths and higher carrier mobility in the rubrene crystals that allow for more effective free carrier generation and collection[18]. Additionally, fabrication of thinner rubrene single crystals than 250 nm by PVT is difficult owing to random producing process, challenging transfer to substrate and not large enough to use in vertical solar cell because of getting anode contact. Our result could be offering a proof of concept of large area single crystal for organic photovoltaic devices. The thickness-optimized single crystal device could be as a powerful platform to compare to differing polycrystalline and amorphous rubrene films and characterize the effect of molecular packing and crystallinity on recombination mechanism. To match the fabrication steps of the single crystal device, a 250 nm rubrene layer was thermally evaporated onto the PCBM layer (**Figure S2**). The as-deposited layer represented the amorphous, and subsequently crystallized through abrupt thermal annealing without de-wetting. This annealing carried out by placing as deposited rubrene films on a pre-heated hot plate in a nitrogen environment. Amorphous surfaces were

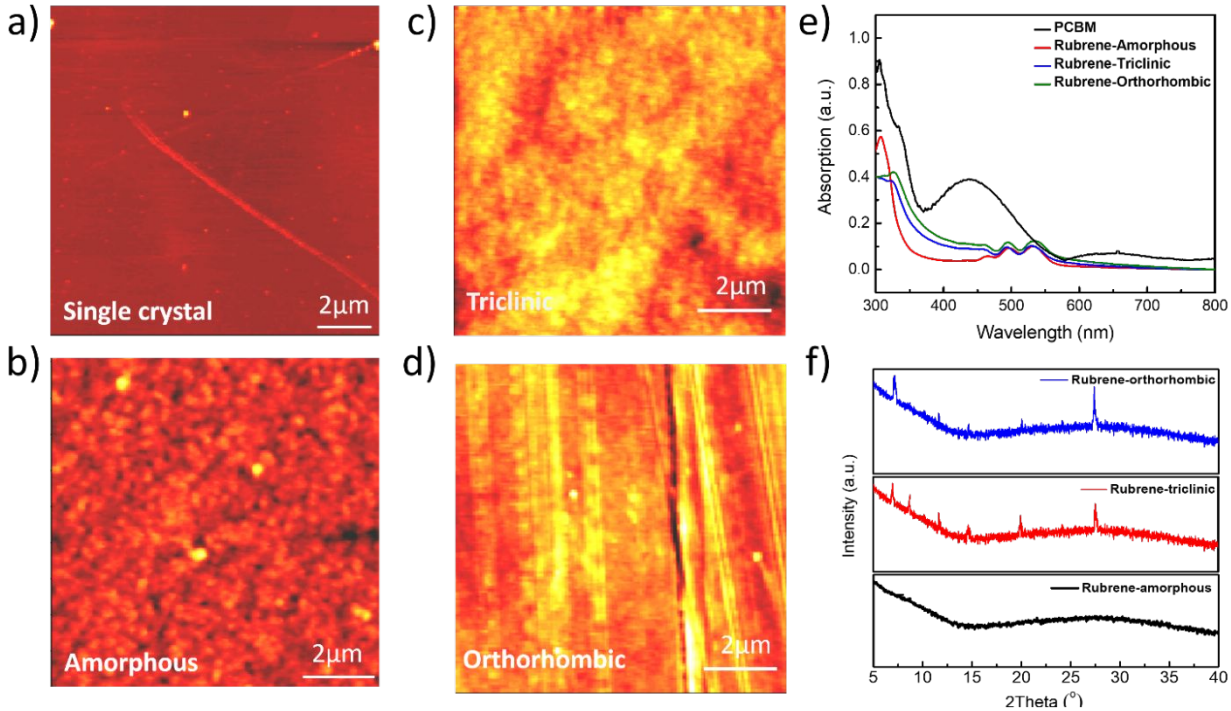

Figure 3. 10 μmx10 μm atomic force microscopy images of 250 nm (a) rubrene single crystal, (b) rubrene-amorphous, (c) rubrene-triclinic and (d) rubrene-orthorhombic surface on PCBM. Absorption spectra and XRD results. e) The absorption in PCBM, rubrene-amorphous, rubrene-triclinic, rubrene-orthorhombic films as a function of wavelength. f) X ray diffraction of amorphous, triclinic, and orthorhombic polymorphs of rubrene

annealed at 130˚C for 5 minutes and 170 ˚C for 3 minutes to fabricate polycrystalline triclinic and orthorhombic films, respectively. Addition to silver metal contact, we deposited MoO_x to fabricate inverted bilayer organic solar cell to achieve better hole collection and get rid of little cracks upon annealing of rubrene which can restrain device operation. To understand the topological variation between the single crystal, polycrystal and amorphous forms of rubrene, we have realized the atomic force microscopy (AFM) measurements. **Figure 3a** shows the image of 250 nm single crystalline rubrene with just single terrace has a smooth and uniform surface exhibiting a monomolecular step which is compossed of rubrene single crystal on c axis[19]. Evolution of crystalline structures upon heat treatment, we examined amorphous and triclinic-polycrystalline and orthothombic polycrystalline features. **Figure 3b** shows the AFM image of amorphous rubrene surface did not exhibit any crystalline feature. After abrupt heating at a relatively low temperature of 130 ˚C for 5 min, disc-shaped crystalline features displayed indicating that homogeneous covered crystalline surfaces as shown in **Figure 3c**[20]. **Figure 3d** shows the orthorhombic crystallized surface of rubrene film on PCBM after thermal heating at 170 ˚C. In there, orthorhombic crystals were oriented with c-axis perpendicular to the substrate[10, 21-22]. Growth-rate of crystal grains and also thickness of the film effect the crystallization type[23-24]. At higher annealing temperatures, circular crystals are reinforcing the transition to the branch-like crystals[9] as seen in **Figure 3d**. Surface profile mapping and 3D surface imaging of amorphous and triclinic-polycrystalline and orthothombic polycrystalline features are illustrated in **Figure S3.** Furthermore, the absorption spectra of PCBM and rubrene polymorphs films and X-ray diffraction peaks of rubrene amorphous, rubrene-triclinic and rubrene-orthorhombic polycrystalline forms have been investigated as shown in **Figure 3e-f.** As can be seen in **Figure 3e**, the PCBM had an absorption peak maximum at 445 nm and characteristic absorption at approximately 300 nm. PCBM/Rubrene triclinic interface show same absorption spectra which is stronger than PCBM/rubrene-orthorhombic. The rubrene amorphous/triclinic and orthorhombic polymorphous forms show similar absorption response and they exhibited an absorption range 475-545 nm with an edge of 575nm. PCBM/Rubrene-Orthorhombic and PCBM/Rubrene triclinic interface show nearly same absorption spectra which is stronger than PCBM/rubrene-amorphous **(Figure S4).** This result is representing an improvement over photocurrent of PCBM/ Rubrene-Orthorhombic and PCBM/Rubrene triclinic bilayer systems. XRD pattern of rubrene polymorphs can be seen in **Figure.3f**. XRD result of rubrene-amorphous film exhibits only glass background signal. The XRD peaks of rubrene-triclinic and rubrene orthorhombic crystalline grains corresponding to characteristic peaks[25-26] which is determined by general structure analysis system (GSAS)[27] and taking the standard CMCA setting[28-29].

Photovoltaic device performances and parameters have been investigated in ITO/C60-N/PCBM/Rubrene/MoOx/Ag for different systems with rubrene crystalline forms. Illuminated

Table 1: Solar cell device parameters fabricated using 250 nm of rubrene as a single crystal, polycrystalline (triclinic-orthorhombic) and amorphous forms.

Device	V_{OC} (mV)	J_{SC} (mA/cm^2)	FF	PCE (%)
250 nm /Single crystalline	600	0.31	0.57	0.11
250 nm/ polycrystalline orthorhombic	730	1.07	0.38	0.29
250 nm/polycrystalline triclinic	790	0.81	0.54	0.35
250 nm/amorphous	880	0.64	0.48	0.27

and dark J-V characteristics are shown in **Figure 4a-b** and the photovoltaic device parameters have been summarized in **Table 1.** Open circuit voltage (V_{OC}) and short circuit current (Jsc) are extracted from illuminated J-V data. The V_{OC} has changed from 880 mV for amorphous rubrene to 600 mV for single crystalline rubrene. It is well known that, HOMO (Highest Occupied Moleculer Orbital) level of amorphous-rubrene is deeper than HOMO level of Rubrene single crystal (about 0.4 eV). Since V_{OC} of organic solar cell found to calculating difference between HOMO level of donor and LUMO level (lowest unoccupied molecular orbital) of the acceptor, a part of this V_{OC} drop can be explained with distinction between HOMO energy levels of amorhous and single crystalline form [30-33]. The single crystalline rubrene V_{OC} which is acquired in this work matched very similar to that of Rand and coworkers[10] and there homoepitaxially grown rubrene layer. On the other hand, the V_{OC} trend of the polycrystalline and amorphous devices follow the similar trend previously reported by Amassian and coworkers [11] in which saw a decrease in V_{OC} from amorphous, triclinic, to orthorhombic in that order. Annealing of donor layers which are rather thick can cause such an abrupt decreasing of V_{OC}. In addition, increased crystalline forms lead to energetically modification of charge transfer state of donor/acceptor interface and effect the fermi energy levels splitting resulted in V_{OC} variation[11, 34]. Besides, it is known that V_{OC} as a device parameter is impressed from recombination mechanisms especially non-radiative recombination existing in device which is discussed in depth at light intensity section[35]. According to overall performance of rubrene based solar cells, PCE results of single crystal devices are still lower than the evaporated rubrene thin film devices because of higher transparency of thin crystals. On the other hand, Jsc, V_{OC} and FF variations for rubrene based organic solar cells need to be explained by charge recombination mechanism in terms of limiting charge collection systems[36]. Recombination in organic solar cells is mostly nonlinear in charge-carrier density[37-38] and therefore device parameters depending on the light intensity, is frequently used in the assay of bimolecular recombination in the field of organic photovoltaics[39-41]. Because of these reasons, in our work, to clarify the performance variation between the single crystal/polymorphs/amorphous solar cells, recombination mechanism at rubrene/PCBM interface have been investigated using the light intensity dependence of J-V characteristics. In **Figure S5,** the J-V behaviour of devices under diffrerent light intensities (ranging from 10 mW/cm^2 to 140 mW/cm^2) were exhibited. Using these J-V graphs of solar cells, we have exracted the solar cell parameters such as open circuit voltage (V_{OC}), short circuit current (J_{SC}), and fill factor (FF) for each light intensity to analyze the charge carrier recombination. It is very well accepted that, at open circuit condition, all the photogenerated charge carries are balanced, and net total current is zero in solar cell devices. In this case, the recombination mechanism can be determined by the following equation[42],

$$Voc \propto n\frac{kT}{q} In\,(I)$$

where q is the elementary charge, k is the Boltzmann's constant, T is temperature in Kelvin and n is the ideality factor introducing the dominant type of recombination mechanism. The linearity of V_{OC} versus the light intensity (log) graph, (the slope is equal to kT/q (n=1)) represents bimolecular recombination whereas stronger dependency of V_{OC} on light intensity refer to presence of another additional recombination mechanism such as trap assisted, which is termed monomolecular recombination. **Figure 4c** displays the V_{OC} value varies with light intensity in there the slope is 1.56 kT/q, 1.66 kT/q, 1.77 kT/q and 2.02 kT/q for single crystal, orthorhombic, triclinic, and amorphous, respectively. The stronger dependence of V_{OC} on light intensity ($1<n<2$) implies a superposition of monomolecular and bimolecular recombination[43]. For amorphous rubrene solar cell device, the slope value reaches to 2.02 kT/q, indicating that trap-assisted mechanism is mostly involved which can be defined by free electron and hole prefer to recombine through trap state or recombination centre, resulting from interfacial defects and impurities in materials[44]. The slope values of orthorhombic and Triclinic crystal employed devices indicate weaker V_{OC} dependence on light intensity than amorphous rubrene based solar cells. These crystal forms might reduce the density of interfacial defects between donor and acceptor layers resulting charge carriers to escape deep traps and decrease trap assisted recombination in comparison with amorphous layer. The value of 1.56 kt/q of single crystal solar cell device demonstrating likely low SRH recombination involved in comparison with amorphous/polymorphous

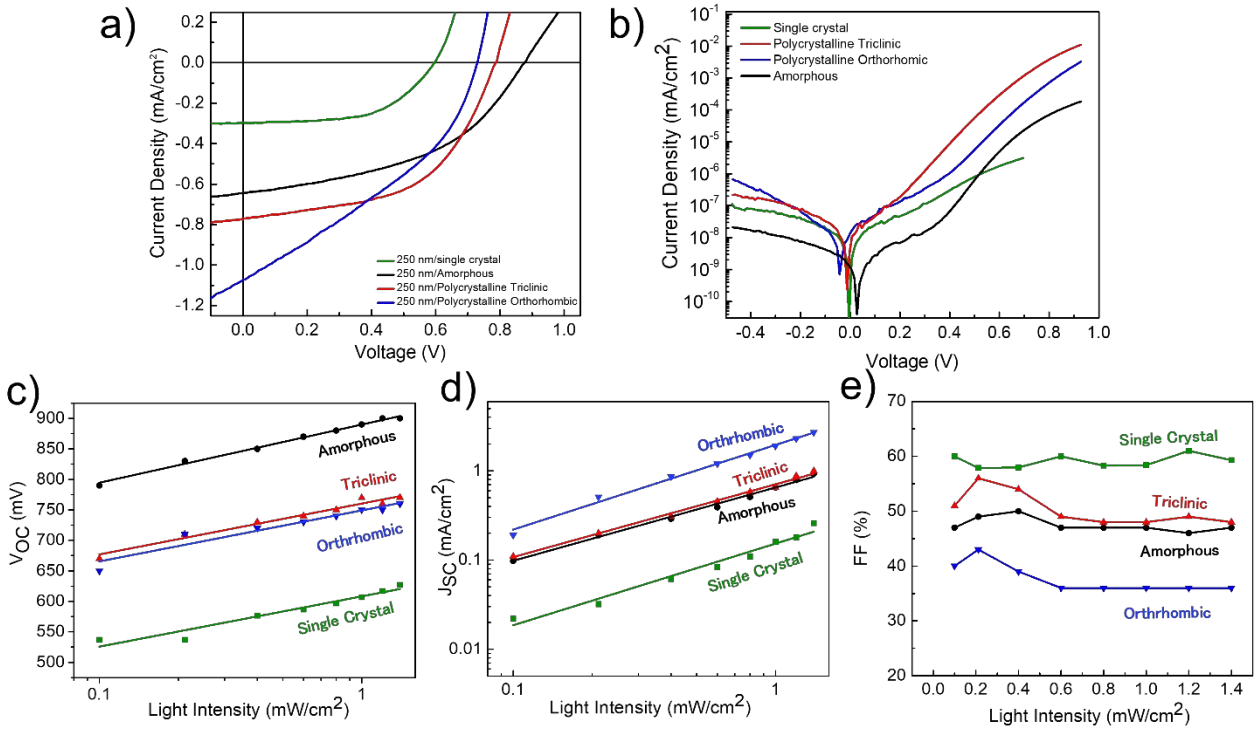

Figure 4.(a) Illuminated and (b) dark J-V characteristics of PCBM/rubrene bilayer devices fabricated using 250 nm of rubrene as a single crystal (green), amorphous (black), polycrystalline triclinic (red), or polycrystalline orthorhombic (blue) film. The light intensity dependence of (c) V_{OC}, (d) J_{SC} and (e) FF of rubrene as a single crystal (green), amorphous (black), polycrystalline triclinic (red), or polycrystalline orthorhombic (blue) film.

counterpart could be resulting of rather low trap assisted behaviour at interface. This situation give rise to less V_{OC} loss caused from non-radiative recombination[35]. It is confirming that, low V_{OC} of single crystal device is resulting from small energy levels splitting instead of bigger non radiative recombination loss due to rubrene single crystals has almost no defects providing long exciton diffusion length[34]. To improve our understanding about charge recombination kinetics, we need to investigate the dependence of FF and J_{SC} on light intensity. The J_{SC} value imply charge carrier collection and transport between absorber layer and electrodes[45-46]. In **Figure 4d**, from the slope of the J_{SC} versus light intensity graph in log-log scale, we extracted the linearity values for single crystal and different formed solar cell devices (amorphous, triclinic, and orthorhombic). For single crystal solar cell, the linearity yield α= 0.93 and α decreases to 0.92, 0.81 and 0.82 for the devices with orthorhombic, triclinic, and amorphous, respectively. These values exhibit the monomolecular (trap assisted) recombination at short circuit conditions but the deep understanding and analysis of J_{SC} variations require both electrical and optical characterization whereas we concentrated on electrical characterizations. That is why, we interpretated the dependency of FF to understand the performance limiting mechanism in solar cell devices. The FF as a function of light can inform about defect states at bulk and interfaces[47]. **Figure 4e** shows the FF versus light intensity graphs of devices. FF values of single crystal device did not change with light intensity where trap assisted recombination is nearly not present. For amorphous rubrene based devices, FF behaviour represents the intermediate bulk recombination or medium interface recombination meaning of trap assisted recombination is the dominant for this type of solar cells. Orthorhombic and triclinic forms of rubrene employed devices exhibits the strong FF dependency under different intensity that can be explained high interface defect densities.

4. Conclusions

In conclusion, organic single crystals with different crystal thickness from 250 nm to 1000 nm were used to fabricate inverted bilayer heterojunction solar cell of rubrene single crystals and PCBM films. The best photovoltaic performance is achieved with 250 nm thick rubrene crystal and it shows PCE of %0.1 with a short-circuit current density of 0.30 mA/cm^2, an open-circuit voltage of 0.60 V, a fill factor of 0.57. Yet, the efficiency of single crystal solar cell is not comparable with thin film devices, these results could be useful for further optoelectronic applications. To our knowledge this is the first time that vertical single crystal solar cell with different rubrene thickness (fabricated by PVT) has been reported. To compare the crystallinity effect on photovoltaic device performance, we have fabricated polycrystalline triclinic orthorhombic, and amorphous bilayer devices which are same thickness of donor layer with single crystal devices. Open circuit voltage of devices

shows a decreasing trend with from amorphous, triclinic, orthorhombic and single crystal. Short circuit current of devices exhibits tendency to inrease from amorphous, triclinic, orthorhombic forms of rubrene based solar cells. According to our results, trilinic form of rubrene show the highest PCE in this device concept. To deeply verify the reason of device parameters changing upon crystalline and ordered surfaces, detailed light intensity measuremet have been realized. The single crystal device shows largely of bimoleculer recombination but amorphous and polycrystalline rubrene based devices shows approximately %30 higher additional monomoleculer recombination which is dominated by trap states. Although the single crystal devices show relatively trap free donor layer and better FF, exhibit still lower PCE than the evaporated rubrene thin film devices because of higher transparency of thin Rubrene crystals.

Author Contributions

Duygu Akin Kara: Conceptualization, Methodology, Data curation, Formal analysis, writing original draft, **Edmund K. Burnett:** Data curation**,** Writing original draft, **Koray Kara:** investigation, and Methodology, **Ozlem Usluer** and **Benjamin P. Cherniawsk**i: Validation, Conceptualization, **Edward J. Barron III**: Methodology**, Burak Gultekin**, **Mahmut Kus** and **Alejandro L. Briseno** :Resources, Project administration, Supervision.

Conflicts of interest

In accordance with our policy on Conflicts of interest please ensure that a conflicts of interest statement is included in your manuscript here. Please note that this statement is required for all submitted manuscripts. If no conflicts exist, please state that “There are no conflicts to declare”.

Acknowledgements

D.A.K. thank to Turkey research fellowship (TUBITAK 2214/A-1059B141501315). K.K. thank to Turkey Scholarship Council (2214/A -1059B141501316). B. G acknowledge the 1003 - Primary Subjects R&D Funding Program (218M940) and A.L.B. acknowledge the Office of Naval Research (N00014-16-1-2612 and N000147-14-1-0053).

Notes and references

1. Kepler, R. G.; Bierstedt, P. E.; Merrifield, R. E., Electronic Conduction and Exchange Interaction in a New Class of Conductive Organic Solids. *Physical Review Letters* **1960,** *5* (11), 503-504.

2. Warta, W.; Karl, N., Hot holes in naphthalene: High, electric-field-dependent mobilities. *Physical Review B* **1985,** *32* (2), 1172-1182.

3. Podzorov, V., Organic single crystals: Addressing the fundamentals of organic electronics. *MRS Bulletin* **2013,** *38* (1), 15-24.

4. Sundar, V. C.; Zaumseil, J.; Podzorov, V.; Menard, E.; Willett, R. L.; Someya, T.; Gershenson, M. E.; Rogers, J. A., Elastomeric transistor stamps: reversible probing of charge transport in organic crystals. *Science (New York, N.Y.)* **2004,** *303* (5664), 1644-6.

5. Podzorov, V.; Sysoev, S. E.; Loginova, E.; Pudalov, V. M.; Gershenson, M. E., Single-crystal organic field effect transistors with the hole mobility ~8 cm2/V s. *Applied Physics Letters* **2003,** *83* (17), 3504-3506.

6. Gershenson, M. E.; Podzorov, V.; Morpurgo, A. F., Colloquium: Electronic transport in single-crystal organic transistors. *Reviews of Modern Physics* **2006,** *78* (3), 973-989.

7. Karak, S.; Lim, J. A.; Ferdous, S.; Duzhko, V. V.; Briseno, A. L., Photovoltaic Effect at the Schottky Interface with Organic Single Crystal Rubrene. *Advanced Functional Materials* **2014,** *24* (8), 1039-1046.

8. Hsu, C. H.; Deng, J.; Staddon, C. R.; Beton, P. H., Growth front nucleation of rubrene thin films for high mobility organic transistors. *Applied Physics Letters* **2007,** *91* (19), 193505.

9. Fielitz, T. R.; Holmes, R. J., Crystal Morphology and Growth in Annealed Rubrene Thin Films. *Crystal Growth & Design* **2016,** *16* (8), 4720-4726.

10. Verreet, B.; Heremans, P.; Stesmans, A.; Rand, B. P., Microcrystalline Organic Thin-Film Solar Cells. *Advanced Materials* **2013,** *25* (38), 5504-5507.

11. Ndjawa, G. O. N.; Graham, K. R.; Mollinger, S.; Wu, D. M.; Hanifi, D.; Prasanna, R.; Rose, B. D.; Dey, S.; Yu, L.; Brédas, J.-L.; McGehee, M. D.; Salleo, A.; Amassian, A., Open-Circuit Voltage in Organic Solar Cells: The Impacts of Donor Semicrystallinity and Coexistence of Multiple Interfacial Charge-Transfer Bands. *Advanced Energy Materials* **2017,** *7* (12), 1601995.

12. Kanashima, T.; Okuyama, M., P(VDF-TeFE)/Organic Semiconductor Structure Ferroelectric-Gate FETs. In *Ferroelectric-Gate Field Effect Transistor Memories: Device Physics and Applications*, Park, B.-E.; Ishiwara, H.; Okuyama, M.; Sakai, S.; Yoon, S.-M., Eds. Springer Netherlands: Dordrecht, 2016; pp 187-201.

13. Agostinelli, G.; Dunlop, E. D.; Batzner, D. L.; Tiwari, A. N.; Nollet, P.; Burgelman, M.; Kontges, M. In *Light dependent current transport mechanisms in chalcogenide solar cells*, 3rd World Conference onPhotovoltaic Energy Conversion, 2003. Proceedings of, 11-18 May 2003; 2003; pp 356-359 Vol.1.

14. Baran, D.; Kirchartz, T.; Wheeler, S.; Dimitrov, S.; Abdelsamie, M.; Gorman, J.; Ashraf, R. S.; Holliday, S.; Wadsworth, A.; Gasparini, N.; Kaienburg, P.; Yan, H.; Amassian, A.; Brabec, C. J.; Durrant, J. R.; McCulloch, I., Reduced voltage losses yield 10% efficient fullerene free organic solar cells with >1 V open circuit voltages. *Energy & Environmental Science* **2016,** *9* (12), 3783-3793.

15. Irkhin, P.; Biaggio, I., Direct Imaging of Anisotropic Exciton Diffusion and Triplet Diffusion Length in Rubrene Single Crystals. *Physical Review Letters* **2011,** *107* (1), 017402.

16. Blom, P. W. M.; Mihailetchi, V. D.; Koster, L. J. A.; Markov, D. E., Device Physics of Polymer:Fullerene Bulk Heterojunction Solar Cells. *Advanced Materials* **2007,** *19* (12), 1551-1566.

17. Tseng, R. J.; Chan, R.; Tung, V. C.; Yang, Y., Anisotropy in Organic Single-Crystal Photovoltaic Characteristics. *Advanced Materials* **2008,** *20* (3), 435-438.

18. Lunt, R. R.; Benziger, J. B.; Forrest, S. R., Relationship between Crystalline Order and Exciton Diffusion Length in Molecular Organic Semiconductors. *Advanced Materials* **2010,** *22* (11), 1233-1236.

19. Menard, E.; Marchenko, A.; Podzorov, V.; Gershenson, M. E.; Fichou, D.; Rogers, J. A., Nanoscale Surface Morphology and Rectifying Behavior of a Bulk Single-Crystal Organic Semiconductor. *Advanced Materials* **2006,** *18* (12), 1552-1556.

20. Lee, H. M.; Moon, H.; Kim, H.-S.; Kim, Y. N.; Choi, S.-M.; Yoo, S.; Cho, S. O., Abrupt heating-induced high-quality crystalline rubrene

thin films for organic thin-film transistors. *Organic Electronics* **2011,** *12* (8), 1446-1453.
21. Brady, M. A.; Su, G. M.; Chabinyc, M. L., Recent progress in the morphology of bulk heterojunction photovoltaics. *Soft Matter* **2011,** *7* (23), 11065-11077.
22. Käfer, D.; Ruppel, L.; Witte, G.; Wöll, C., Role of Molecular Conformations in Rubrene Thin Film Growth. *Physical Review Letters* **2005,** *95* (16), 166602.
23. Kim, J. H.; Jang, J.; Zin, W.-C., Thickness Dependence of the Glass Transition Temperature in Thin Polymer Films. *Langmuir* **2001,** *17* (9), 2703-2710.
24. Yu, L., Surface mobility of molecular glasses and its importance in physical stability. *Advanced drug delivery reviews* **2016,** *100*, 3-9.
25. Pascoe, A. R.; Gu, Q.; Rothmann, M. U.; Li, W.; Zhang, Y.; Scully, A. D.; Lin, X.; Spiccia, L.; Bach, U.; Cheng, Y.-B., Directing nucleation and growth kinetics in solution-processed hybrid perovskite thin-films. *SCIENCE CHINA Materials* **2017,** *60* (2095-8226), 617.
26. Huang, L.; Liao, Q.; Shi, Q.; Fu, H.; Ma, J.; Yao, J., Rubrene micro-crystals from solution routes: their crystallography, morphology and optical properties. *Journal of Materials Chemistry* **2010,** *20* (1), 159-166.
27. Larson, a.; Von Dreele, R. B., GSAS-GENERAL STRUCTURE ANALYSIS SYSTEM. The Regents of the University of California: 1985-1994; Vol. LAUR 86-748.
28. Chapman, B. D.; Checco, A.; Pindak, R.; Siegrist, T.; Kloc, C., Dislocations and grain boundaries in semiconducting rubrene single-crystals. *Journal of Crystal Growth* **2006,** *290* (2), 479-484.
29. Jurchescu, O. D.; Meetsma, A.; Palstra, T. T. M., Low-temperature structure of rubrene single crystals grown by vapor transport. *Acta Crystallographica Section B* **2006,** *62* (2), 330-334.
30. Rand, B. P.; Burk, D. P.; Forrest, S. R., Offset energies at organic semiconductor heterojunctions and their influence on the open-circuit voltage of thin-film solar cells. *Physical Review B* **2007,** *75* (11), 115327.
31. Ueba, T.; Park, J.; Terawaki, R.; Watanabe, Y.; Yamada, T.; Munakata, T., Unoccupied electronic structure and molecular orientation of rubrene; from evaporated films to single crystals. *Surface Science* **2016,** *649*, 7-13.
32. Wang, K.; Ecker, B.; Gao, Y., Angle-Resolved Photoemission Study on the Band Structure of Organic Single Crystals. *Crystals* **2020,** *10* (9), 773.
33. Nakayama, Y.; Iwashita, M.; Kikuchi, M.; Tsuruta, R.; Yoshida, K.; Gunjo, Y.; Yabara, Y.; Hosokai, T.; Koganezawa, T.; Izawa, S.; Hiramoto, M., Electronic and Crystallographic Examinations of the Homoepitaxially Grown Rubrene Single Crystals. *Materials* **2020,** *13* (8), 1978.
34. Nakayama, Y.; Machida, S.; Minari, T.; Tsukagishi, K.; Noguchi, Y.; Ishii, H., Direct observation of the electronic states of single crystalline rubrene under ambient condition by photoelectron yield spectroscopy. *Applied Physics Letters* **2008,** *93* (17), 173305.
35. Street, R. A.; Krakaris, A.; Cowan, S. R., Recombination Through Different Types of Localized States in Organic Solar Cells. *Advanced Functional Materials* **2012,** *22* (21), 4608-4619.
36. Hartnagel, P.; Kirchartz, T., Understanding the Light-Intensity Dependence of the Short-Circuit Current of Organic Solar Cells. *Advanced Theory and Simulations* **2020,** *3* (10), 2000116.
37. Dibb, G. F. A.; Kirchartz, T.; Credgington, D.; Durrant, J. R.; Nelson, J., Analysis of the Relationship between Linearity of Corrected Photocurrent and the Order of Recombination in Organic Solar Cells. *The Journal of Physical Chemistry Letters* **2011,** *2* (19), 2407-2411.
38. Credgington, D.; Durrant, J. R., Insights from Transient Optoelectronic Analyses on the Open-Circuit Voltage of Organic Solar Cells. *The Journal of Physical Chemistry Letters* **2012,** *3* (11), 1465-1478.
39. Koster, L. J. A.; Mihailetchi, V. D.; Xie, H.; Blom, P. W. M., Origin of the light intensity dependence of the short-circuit current of polymer/fullerene solar cells. *Applied Physics Letters* **2005,** *87* (20), 203502.
40. Zhao, F.; Dai, S.; Wu, Y.; Zhang, Q.; Wang, J.; Jiang, L.; Ling, Q.; Wei, Z.; Ma, W.; You, W.; Wang, C.; Zhan, X., Single-Junction Binary-Blend Nonfullerene Polymer Solar Cells with 12.1% Efficiency. *Advanced materials (Deerfield Beach, Fla.)* **2017,** *29* (18).
41. Fan, Q.; Su, W.; Wang, Y.; Guo, B.; Jiang, Y.; Guo, X.; Liu, F.; Russell, T. P.; Zhang, M.; Li, Y., Synergistic effect of fluorination on both donor and acceptor materials for high performance non-fullerene polymer solar cells with 13.5% efficiency. *Science China Chemistry* **2018,** *61* (5), 531-537.
42. Cowan, S. R.; Roy, A.; Heeger, A. J., Recombination in polymer-fullerene bulk heterojunction solar cells. *Physical Review B* **2010,** *82* (24), 245207.
43. Tress, W.; Yavari, M.; Domanski, K.; Yadav, P.; Niesen, B.; Correa Baena, J. P.; Hagfeldt, A.; Graetzel, M., Interpretation and evolution of open-circuit voltage, recombination, ideality factor and subgap defect states during reversible light-soaking and irreversible degradation of perovskite solar cells. *Energy & Environmental Science* **2018,** *11* (1), 151-165.
44. An, Q.; Zhang, F.; Sun, Q.; Zhang, M.; Zhang, J.; Tang, W.; Yin, X.; Deng, Z., Efficient organic ternary solar cells with the third component as energy acceptor. *Nano Energy* **2016,** *26*, 180-191.
45. Lenes, M.; Morana, M.; Brabec, C. J.; Blom, P. W. M., Recombination-Limited Photocurrents in Low Bandgap Polymer/Fullerene Solar Cells. *Advanced Functional Materials* **2009,** *19* (7), 1106-1111.
46. Zhang, Y.; Dang, X.-D.; Kim, C.; Nguyen, T.-Q., Effect of Charge Recombination on the Fill Factor of Small Molecule Bulk Heterojunction Solar Cells. *Advanced Energy Materials* **2011,** *1* (4), 610-617.
47. Glowienka, D.; Galagan, Y., Light Intensity Analysis of Photovoltaic Parameters for Perovskite Solar Cells. *Advanced Materials n/a* (n/a), 2105920.